Proceedings of IMECE2008
2008 ASME International Mechanical Engineering Congress and Exposition
October 31-November 6, 2008, Boston, Massachusetts, USA

IMECE2008-67335

ADVANCED FINITE ELEMENT FORMULATION FOR PIEZOELECTRIC SMART SHELL STRUCTURES UNDER CONSIDERATION OF GEOMETRICAL NONLINEARITY

Katrin Schulz*
Institut für Baustatik
Universität Karlsruhe (TH)
76131 Karlsruhe, Germany
Email: katrin.schulz@bs.uni-karlsruhe.de

Sven Klinkel
Werner Wagner
Institut für Baustatik
Universität Karlsruhe (TH)
76131 Karlsruhe, Germany

ABSTRACT

A geometrically nonlinear highly accurate finite element formulation to analyze piezoelectric shell problems is presented. The formulation is based on the mixed field variational principle of Hu-Washizu including the independent fields displacements, electric potential, strains, electric field, mechanical stresses and dielectric displacements. The normal zero stress condition and the normal zero dielectric displacement condition for shells are enforced by the independent resultant stress and resultant dielectric displacement fields. The arbitrary reference surface of the shell is modeled with a four node element. Each node possesses six mechanical degrees of freedom, three displacements and three rotations, and one electrical degree of freedom, which is the difference of the electric potential through the shell thickness. The developed shell element fulfills the patchtests and is able to model arbitrary curved shell structures. Some numerical examples demonstrate the applicability of the present shell element for piezoelectric systems and integrated piezoelectric structures.

INTRODUCTION

Smart materials and structures play an important role for sensor and actuator applications, as high precision systems, valves, the vibration control or the measurement of expansion or acceleration. For the simulation of such systems it is essential to predict the material and system behavior in a numerical model as precisely as possible. A reliable simulation may provide an easier, faster and cheaper development of such devices.

Hence, this paper is concerned with a geometrically nonlinear highly accurate finite element formulation to analyze piezoelectric shell problems. Therefore the classical shell assumptions are extended to the electromechanical coupled field problem. The formulation is based on the mixed field variational principle of Hu-Washizu including the independent fields displacements, electric potential, strains, electric field, mechanical stresses and dielectric displacements. The mixed formulation allows an interpolation of the strains and the electric field through the shell thickness, which is an essential advantage when using a three-dimensional material law. Thus, the formulation allows the consideration of arbitrary nonlinear constitutive relations. Here, a linear constitutive relation is employed. It is remarked that no simplification regarding the constitutive law is assumed. The normal zero stress condition, which is a common assumption in shell theories, and the normal zero dielectric displacement condition are enforced by the independent resultant stress and resultant dielectric displacement fields.

The trend goes to more and more thinner structures, that is, shell structures. In recent years some piezoelectric shell elements have been proposed. One may distinguish between surface oriented models, e.g. [1], and shell elements with respect to a reference surface, e.g. [2], [3]. Here the shell structure is modeled

*Address all correspondence to this author.

by a reference surface with a four node element. Each node possesses six mechanical degrees of freedom, three displacements and three rotations, and one electrical degree of freedom, which is the difference of the electric potential in thickness direction. An appropriate interpolation of the independent stress, strain, dielectric displacement and electric field are presented.

The developed shell element fulfills the patch tests, the in-plane, bending and shear test, which have been adopted for coupled field problems, and is able to model arbitrary curved shell structures. Some numerical examples demonstrate the applicability of the present shell element for piezoelectric systems and integrated piezoelectric structures. Furthermore some practical devices, as for example a smart antenna, are analyzed.

KINEMATICS

The Green-Lagrangean strains are arranged in the vector $\mathbf{E}_g = \left[\varepsilon_{11}\ \varepsilon_{22}\ \varepsilon_{33}\ 2\varepsilon_{12}\ 2\varepsilon_{13}\ 2\varepsilon_{23}\right]$. The coefficients of the strain vector are defined as the gradient field

$$\mathbf{E}_g = \frac{1}{2}(grad\, u + grad^T u + grad^T u\ grad\, u), \tag{1}$$

where u is the displacement vector. The components of the vector of the geometric electric field $\vec{\mathbf{E}} = \left[\vec{E}_1\ \vec{E}_2\ \vec{E}_3\right]$ are given by

$$\vec{\mathbf{E}}_g = -grad\, \Delta\varphi \tag{2}$$

where $\Delta\varphi$ denotes the electric potential. The electric field is also derived in convective coordinates. The gradient refers to the reference configuration.

CONSTITUTIVE EQUATIONS

We write the constitutive relations, according to Voigt's linear piezoelectricity theory, see e.g. Voigt [4] as

$$\underbrace{\begin{bmatrix}\mathbf{S}\\ -\vec{\mathbf{D}}\end{bmatrix}}_{\sigma} = \underbrace{\begin{bmatrix}\mathbb{C} & -\mathbb{e}^T\\ -\mathbb{e} & -\varepsilon_s\end{bmatrix}}_{\bar{\mathbb{C}}}\underbrace{\begin{bmatrix}\mathbf{E}\\ \vec{\mathbf{E}}\end{bmatrix}}_{\varepsilon} \tag{3}$$

$\bar{\mathbb{C}}$ here describes the constant material matrix consisting of the three dimensional simplified isotropic elasticity matrix $\mathbb{C}$ with Young's modulus E and Poisson ratio ν

$$\mathbb{C} = \frac{E}{(1+\nu)(1-2\nu)}\begin{bmatrix} 1-\nu & \nu & \nu & 0 & 0 & 0\\ \nu & 1-\nu & \nu & 0 & 0 & 0\\ \nu & \nu & 1-\nu & 0 & 0 & 0\\ 0 & 0 & 0 & \frac{1-2\nu}{2} & 0 & 0\\ 0 & 0 & 0 & 0 & \frac{1-2\nu}{2} & 0\\ 0 & 0 & 0 & 0 & 0 & \frac{1-2\nu}{2}\end{bmatrix} \tag{4}$$

as well as the piezoelectric matrix $\mathbb{e}$ and the permittivity matrix ε_s

$$\mathbb{e}^T = \begin{bmatrix} 0 & 0 & e_{13}\\ 0 & 0 & e_{13}\\ 0 & 0 & e_{33}\\ 0 & 0 & 0\\ e_{15} & 0 & 0\\ 0 & e_{15} & 0\end{bmatrix} \qquad \varepsilon_s = \begin{bmatrix}\varepsilon_{11} & 0 & 0\\ 0 & \varepsilon_{11} & 0\\ 0 & 0 & \varepsilon_{33}\end{bmatrix} \tag{5}$$

The strains $\mathbf{E}$ and the electric field $\vec{\mathbf{E}}$ can be arranged in the generalized vector ε as well as the second Piola-Kichhoff stresses $\mathbf{S}$ and the material dielectric displacements $\vec{\mathbf{D}}$ in the vector σ.
In order to connect the quantities of the shell with those of the continuum we introduce a matrix $\mathbf{A}$.

$$\mathbf{A} = \begin{bmatrix}
1&0&0&\xi^3&0&0&0&0&0&0&0&0&0&0\\
0&1&0&0&\xi^3&0&0&0&0&0&0&0&0&0\\
0&0&0&0&0&0&0&0&0&0&1&\xi^3&0&0\\
0&0&1&0&0&\xi^3&0&0&0&0&0&0&0&0\\
0&0&0&0&0&0&1&0&0&0&0&0&0&0\\
0&0&0&0&0&0&0&1&0&0&0&0&0&0\\
0&0&0&0&0&0&0&0&1&0&0&0&0&0\\
0&0&0&0&0&0&0&0&0&1&0&0&0&0\\
0&0&0&0&0&0&0&0&0&0&0&1&\xi^3
\end{bmatrix} \tag{6}$$

This matrix transforms the strains and the electric field of the shell $\bar{\varepsilon}$ into the continuum vector ε

$$\varepsilon = A\bar{\varepsilon} \tag{7}$$

The vector $\bar{\varepsilon}$ has the form

$$\bar{\varepsilon} = \left[\varepsilon_{11}\ \varepsilon_{22}\ 2\varepsilon_{12}\ \kappa_{11}\ \kappa_{22}\ 2\kappa_{12}\ \gamma_1\ \gamma_2\ \vec{E}_1\ \vec{E}_2\ \varepsilon^0_{33}\ \varepsilon^1_{33}\ \vec{E}^m_3\ \vec{E}^b_3\right]^T \tag{8}$$

$$= \left[\varepsilon_p\ \varepsilon_z\right]^T \tag{9}$$

Herein ε_p contains the shells strains in the first and second coordinate direction, where the subscript p indicates physical strains

which are related to the constitutive equations. Furthermore the vector ε_z contain the components in thickness direction. ε^0_{33}, ε^1_{33} denote the constant and linear part of the independent thickness strain and $\vec{E}^m_3$, $\vec{E}^b_3$ the membrane and the bending part of the electric field in thickness direction, respectively. The associated variation of the strains reads $\delta\bar{\varepsilon}$.
One obtains the stress resultants of the shell $\mathbf{S}$ from a thickness integration

$$\mathbf{S} = \int_{-\frac{h}{2}}^{\frac{h}{2}} A^T \sigma \, d\xi^3 = \underbrace{\int_{-\frac{h}{2}}^{\frac{h}{2}} A^T \bar{\mathbb{C}} A \, d\xi^3}_{\mathbb{D}} \bar{\varepsilon} \tag{10}$$

where $\mathbb{D}$ denotes the material matrix of the shell. Here we denote σ as stress vector

$$\sigma = [\sigma_{11}, \sigma_{22}, \sigma_{33}, \sigma_{12}, \sigma_{13}, \sigma_{23}, -\vec{D}_1, -\vec{D}_2, -\vec{D}_3]^T \tag{11}$$

The vector of the stress resultants has the form

$$S = [n^{11}, n^{22}, n^{12}, m^{11}, m^{22}, m^{12}, q^1, q^2, -d_1, -d_2, n^{33}_0, n^{33}_1, -d^m_3, -d^b_3]^T \tag{12}$$

with membrane forces $n^{\alpha\beta} = n^{\beta\alpha}$, bending moments $m^{\alpha\beta} = m^{\beta\alpha}$, shear forces q^α and d_α dielectric displacement.

VARIATIONAL FORMULATION

In this section we introduce the functional $\Pi(\mathbf{v}, \Delta\varphi, \hat{\varepsilon}, \hat{\sigma})$, which is based on a Hu-Washizu functional. The formulation has six independent fields, the displacement $\mathbf{v}$, the difference of the electric potential in thickness direction $\Delta\varphi$, the independent vector $\hat{\varepsilon}(\mathbf{E}, \vec{\mathbf{E}})$ and the assumed vector $\hat{\sigma}(\mathbf{S}, \vec{\mathbf{D}})$.

$$\Pi = \int_{\mathcal{B}} W_s(\hat{\varepsilon}) \, dV + \int_{\mathcal{B}} \hat{\sigma}^T (\varepsilon_g - \hat{\varepsilon}) \, dV - \int_{\mathcal{B}} \mathbf{v}^T \mathbf{p} \, dV - \int_{\partial\mathcal{B}_\mathbf{t}} \mathbf{v}^T \mathbf{t} \, dA \tag{13}$$

The stored energy function W_s is defined as $W_s = \frac{1}{2}\hat{\varepsilon}^T \bar{\mathbb{C}} \hat{\varepsilon}$. The vector ε_g contains the geometric strains $\mathbf{E}_g$ and the geometric electric field $\vec{\mathbf{E}}_g$. $\mathbf{p}$ denotes the body force and $\mathbf{t}$ is the prescribed traction vector on the boundary $\partial\mathcal{B}_\mathbf{t}$.
The first variation of Eq.(13) leads to the variational formulation

$$\begin{aligned} \delta\Pi(\mathbf{v}, \Delta\varphi, \hat{\varepsilon}, \hat{\sigma}) = & \int_{\mathcal{B}} \frac{\partial \mathbf{W_s}}{\partial \hat{\varepsilon}} : \delta\hat{\varepsilon} \, dV \\ & + \int_{\mathcal{B}} \partial\hat{\sigma} : (\varepsilon_g - \hat{\varepsilon}) + \hat{\sigma} : \delta\varepsilon_g - \hat{\sigma} : \delta\hat{\varepsilon} \, dV \\ & - \int_{\mathcal{B}} \delta\mathbf{v}^T \mathbf{p} \, dV - \int_{\partial\mathcal{B}_t} \delta\mathbf{v}^T \mathbf{t} \, dA \qquad = 0 \end{aligned} \tag{14}$$

For the vector of the independent stress resultants and the independent dielectric displacement we assume

$$\begin{aligned} \hat{\bar{\mathbf{S}}} &= \begin{bmatrix} n_{11} & n_{22} & n_{12} & m_1 & m_2 & m_{12} & q_1 & q_2 & -d_1 & -d_2 & 0 & 0 & 0 \end{bmatrix}^T \\ &= \begin{bmatrix} \hat{\mathbf{S}} & \underline{0} \end{bmatrix}^T \end{aligned} \tag{15}$$

The stress and dielectric displacement in thickness direction are defined as zero, so we fulfill the normal zero stress condition of shells.
An integration through the thickness of (14) leads to

$$\begin{aligned} \delta\Pi = & \int_\Omega \delta\varepsilon_g^T \hat{\mathbf{S}} - \delta\mathbf{v}^T \bar{\mathbf{p}} \, dA - \int_{\Gamma_\sigma} \delta\mathbf{v}^T \bar{\mathbf{t}} \, ds \\ & + \int_\Omega \delta\hat{\bar{\varepsilon}}^T (\mathbb{D}\hat{\bar{\varepsilon}} - \hat{\bar{\mathbf{S}}}) \, dA \\ & + \int_\Omega \delta\hat{\mathbf{S}}^T (\varepsilon_g - \hat{\varepsilon}) \, dA \qquad = 0 \end{aligned} \tag{16}$$

$\bar{\mathbf{p}}$ describes the body force and $\bar{\mathbf{t}}$ stands for the prescribed traction vector on the boundary Γ_σ. The generalized geometric vector ε_g does not consider the components in thickness direction.

FINITE ELEMENT FORMULATION

We consider a four node quadrilateral shell element with bilinear shape functions N_I

$$N_I(\xi, \eta) = \frac{1}{4}(1 + \xi_I \xi)(1 + \eta_I \eta) \qquad I = 1..4 \tag{17}$$

The shell structure is modeled by a reference surface as shown in Figure 1. Each node has seven degrees of freedom, three lo-

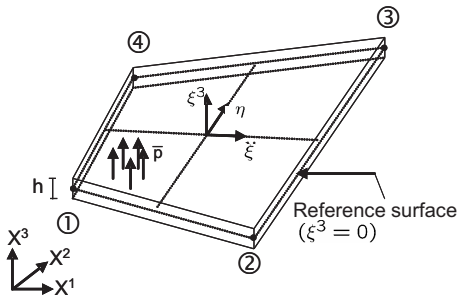

Figure 1. SHELL STRUCTURE MODELED BY A REFERENCE SURFACE

cal displacements, three local rotations, and the difference of the

electric potential in thickness direction. By means of the isoparametric concept the displacements $\mathbf{u}$, the difference of the electric potential $\Delta\varphi$ and the geometry are approximated with the same shape functions.

$$\begin{bmatrix} \mathbf{u}^h \\ \Delta\varphi^h \end{bmatrix} = \sum_{I=1}^{4} \mathbf{N}_I \, \mathbf{v}_I = \mathbf{N} \, \mathbf{v}_e \qquad \text{with } \mathbf{v}_e^T = [\mathbf{v}_1^T \ \mathbf{v}_2^T \ \mathbf{v}_3^T \ \mathbf{v}_4^T] \quad (18)$$

with $\mathbf{v}_I = (u \ v \ w \ \Delta\varphi)_I$. The local numbering of the corner nodes can be seen in Fig.1. A map of the coordinates $\{\xi, \eta\} \in [-1, 1]$ from the unit square to the reference surface in the initial and current configuration is applied. Thus we interpolate the position vector and the director vector of the reference surface with the functions N_I

$$\mathbf{X}^h = \sum_{I=1}^{4} N_I \, \mathbf{X}_I \qquad \mathbf{D}^h = \sum_{I=1}^{4} N_I \, \mathbf{D}_I \qquad (19)$$

The superscript h denotes the characteristic size of the element discretization and indicates the finite element approximation. The nodal position vectors $\mathbf{X}_I$ and the local cartesian basis systems $[\mathbf{A}_{1I}, \mathbf{A}_{2I}, \mathbf{A}_{3I}]$ are generated within the mesh input. Here, $\mathbf{D}_I = \mathbf{A}_{3I}$ is perpendicular to Ω and $\mathbf{A}_{1I}$, $\mathbf{A}_{2I}$ are constructed in such a way that the boundary conditions can be accommodated, see [5].

With the matrix $\mathbf{B}$, which contains the derivations of the shape functions, we obtain the geometric strains and the geometric electric field

$$\begin{bmatrix} \delta\mathbf{E}_g \\ \delta\vec{\mathbf{E}}_g \end{bmatrix} = \sum_{I=1}^{4} \mathbf{B}_I \, \mathbf{v}_I = \mathbf{B} \, \mathbf{v}_e \qquad (20)$$

Interpolations of Strains and Stress Resultants

For the quantities of the strains and the electric field we assume

$$\hat{\bar{\varepsilon}} = \bar{\mathbf{N}}_\varepsilon \, \bar{\alpha}, \qquad \hat{\varepsilon} = \hat{\mathbf{N}}_\varepsilon \, \alpha \qquad (21)$$

$\hat{\bar{\varepsilon}}$ denotes the complete vector of the strains and the electric field whereas $\hat{\varepsilon}$ denotes the vector without the components in thickness direction. The vector of the stress resultants and the dielectric displacement $\hat{\mathbf{S}}$ is given as

$$\hat{\mathbf{S}} = \mathbf{N}_\sigma \, \beta \qquad (22)$$

The vectors $\alpha, \bar{\alpha}$ and β contain independent variables which are eliminated by static condensation on element level.

The matrices $\hat{\mathbf{N}}_\varepsilon, \bar{\mathbf{N}}_\varepsilon$ and $\mathbf{N}_\sigma$ are defined as

$$\hat{\mathbf{N}}_\varepsilon = \begin{bmatrix} \mathbf{N}_\varepsilon & \underline{0} \\ \underline{0} & \mathbf{N}_\sigma^{el} \end{bmatrix} \qquad \mathbf{N}_\varepsilon = \begin{bmatrix} \mathbf{1}_3 & \underline{0} & \underline{0} & \mathbf{N}_\varepsilon^m & \underline{0} & \underline{0} \\ \underline{0} & \mathbf{1}_3 & \underline{0} & \underline{0} & \mathbf{N}_\varepsilon^b & \underline{0} \\ \underline{0} & \underline{0} & \mathbf{1}_2 & \underline{0} & \underline{0} & \mathbf{N}_\varepsilon^s \end{bmatrix}$$

$$\mathbf{N}_\sigma^{el} = \mathbf{J} \begin{bmatrix} 1 & 0 & \tilde{\eta} & 0 \\ 0 & 1 & 0 & \tilde{\xi} \end{bmatrix}$$

$$\bar{\mathbf{N}}_\varepsilon = \begin{bmatrix} \hat{\mathbf{N}}_\varepsilon & \underline{0} & \underline{0} & \mathbf{N}_{eas} \\ \underline{0} & \mathbf{N}_\varepsilon^z & \underline{0} & \underline{0} \\ \underline{0} & \underline{0} & \tilde{\mathbf{N}}_\varepsilon^{el} & \underline{0} \end{bmatrix} \qquad \mathbf{N}_\varepsilon^z = \begin{bmatrix} 1 & \xi & \eta & \xi\cdot\eta & 0 & 0 & 0 & 0 \\ 0 & 0 & 0 & 0 & 1 & \xi & \eta & \xi\cdot\eta \end{bmatrix}$$

$$\tilde{\mathbf{N}}_\varepsilon^{el} = \mathbf{J} \begin{bmatrix} 1 & 0 & \tilde{\xi} & \tilde{\eta} & \tilde{\xi}\cdot\tilde{\eta} & 0 & 0 & 0 \\ 0 & 1 & 0 & 0 & 0 & \tilde{\xi} & \tilde{\eta} & \tilde{\xi}\cdot\tilde{\eta} \end{bmatrix}$$

$$\mathbf{N}_\sigma = \begin{bmatrix} \mathbf{N}_\sigma^{mech} & \underline{0} \\ \underline{0} & \mathbf{N}_\sigma^{el} \end{bmatrix} \qquad \mathbf{N}_\sigma^{mech} = \begin{bmatrix} \mathbf{1}_3 & \underline{0} & \underline{0} & \mathbf{N}_\sigma^m & \underline{0} & \underline{0} \\ \underline{0} & \mathbf{1}_3 & \underline{0} & \underline{0} & \mathbf{N}_\sigma^b & \underline{0} \\ \underline{0} & \underline{0} & \mathbf{1}_2 & \underline{0} & \underline{0} & \mathbf{N}_\sigma^s \end{bmatrix}$$

$\tilde{\xi} = \xi - \bar{\xi}$, $\tilde{\eta} = \eta - \bar{\eta}$. The matrix $\mathbf{N}_{eas}$ contain parameters which are constructed orthogonal to the stress interpolations. This is similar to an enhanced strain formulation.

$$\mathbf{N}_{eas} = \begin{bmatrix} \mathbf{N}_{eas}^m & \underline{0} \\ \underline{0} & \mathbf{N}_{eas}^b \end{bmatrix} \qquad \mathbf{N}_{eas}^m = \mathbf{N}_{eas}^b = \tfrac{j_0}{j} (T_\sigma^0)^{-T} M_\alpha$$

$$M_\alpha = \begin{bmatrix} \xi & 0 & \xi\eta & 0 & 0 & 0 & 0 \\ 0 & \eta & 0 & \xi\eta & 0 & 0 & 0 \\ 0 & 0 & 0 & 0 & \xi & \eta & \xi\eta \end{bmatrix} \qquad \alpha = 2, 4, 7 \qquad (23)$$

For the definition of the matrices $\mathbf{N}_{\varepsilon/\sigma}^m$, $\mathbf{N}_{\varepsilon/\sigma}^b$ and $\mathbf{N}_{\varepsilon/\sigma}^s$ (see also [6]) it holds

$$\mathbf{N}_\varepsilon^m = \mathbf{N}_\varepsilon^b = \mathbf{T}_\varepsilon^0 \begin{bmatrix} \eta - \bar{\eta} & 0 \\ 0 & \xi - \bar{\xi} \\ 0 & 0 \end{bmatrix}, \ \mathbf{T}_\varepsilon^0 = \begin{bmatrix} J_{11}^0 J_{11}^0 & J_{21}^0 J_{21}^0 & J_{11}^0 J_{21}^0 \\ J_{12}^0 J_{12}^0 & J_{22}^0 J_{22}^0 & J_{12}^0 J_{22}^0 \\ 2J_{11}^0 J_{12}^0 & 2J_{21}^0 J_{22}^0 & J_{11}^0 J_{22}^0 + J_{12}^0 J_{21}^0 \end{bmatrix} \qquad (24)$$

$$\mathbf{N}_\sigma^m = \mathbf{N}_\sigma^b = \mathbf{T}_\sigma^0 \begin{bmatrix} \eta - \bar{\eta} & 0 \\ 0 & \xi - \bar{\xi} \\ 0 & 0 \end{bmatrix} \qquad \mathbf{N}_\varepsilon^s = \mathbf{N}_\sigma^s = \tilde{\mathbf{T}}_\sigma^0 \begin{bmatrix} \eta - \bar{\eta} & 0 \\ 0 & \xi - \bar{\xi} \end{bmatrix} \qquad (25)$$

where the matrices

$$\mathbf{T}_\sigma^0 = \begin{bmatrix} J_{11}^0 J_{11}^0 & J_{21}^0 J_{21}^0 & 2J_{11}^0 J_{21}^0 \\ J_{12}^0 J_{12}^0 & J_{22}^0 J_{22}^0 & 2J_{12}^0 J_{22}^0 \\ J_{11}^0 J_{12}^0 & J_{21}^0 J_{22}^0 & J_{11}^0 J_{22}^0 + J_{12}^0 J_{21}^0 \end{bmatrix} \qquad \tilde{\mathbf{T}}_\sigma^0 = \begin{bmatrix} J_{11}^0 & J_{21}^0 \\ J_{12}^0 & J_{22}^0 \end{bmatrix} \qquad (26)$$

describe the transformation of contravariant tensor components to the local cartesian coordinate system at the element center. The constants $J_{\alpha\beta}^0 = J_{\alpha\beta}(\xi = 0, \eta = 0)$ are the components of the

Jacobian matrix **J** evaluated at the element center.
The interpolation of the membrane forces and bending moments, see equation (23) corresponds to the enhanced assumed strain method, introduced in [7] ; Due to the constants

$$\bar{\xi} = \frac{1}{A_e} \int_{(\Omega_e)} \xi \, dA \qquad \bar{\eta} = \frac{1}{A_e} \int_{(\Omega_e)} \eta \, dA \qquad A_e = \int_{(\Omega_e)} dA \tag{27}$$

the linear functions are orthogonal to the constant function which yields partly decoupled matrices. dA describes the area element, $dA = j \, d\xi d\eta$.

Linearized Variational Formulation

We introduce $\theta = [\mathbf{u}, \Delta\varphi, \hat{\varepsilon}, \hat{\sigma}]^T$ and the associated virtual quantities $\delta\theta = [\delta\mathbf{u}, \delta\Delta\varphi, \delta\hat{\varepsilon}, \delta\hat{\sigma}]^T$. The linearization of the variational equation reads

$$L[\delta\Pi(\theta, \delta\theta), \Delta\theta] := \delta\Pi(\theta, \delta\theta) + D(\delta\Pi) \cdot \Delta\theta$$

$$D(\delta\Pi) \cdot \Delta\theta = \int_{(\Omega)} [\delta\varepsilon_g^T \Delta\hat{S} + \Delta\delta\varepsilon_g^T \hat{S} + \delta\hat{\varepsilon}^T (\mathbb{D}\Delta\hat{\varepsilon} - \Delta\hat{\bar{S}}) + \delta\hat{S}^T (\Delta\varepsilon_g - \Delta\hat{\varepsilon})] \, dA$$

Inserting all the interpolations into the variational formulation we derive the linearized expression

$$\begin{aligned}
\delta\Pi_e = {} & \delta\mathbf{v}_e^T \int_{\Omega_e} \left[\mathbf{B}^T \mathbf{N}_\sigma \, \Delta\beta + \mathbf{B}^T \hat{\mathbf{S}} - f^a \right] dA \\
& + \delta\bar{\alpha}^T \int_{\Omega_e} \left[\bar{\mathbf{N}}_\varepsilon^T \mathbb{D} \bar{\mathbf{N}}_\varepsilon \, \Delta\bar{\alpha} \right] dA \\
& - \delta\bar{\alpha}^T \int_{\Omega_e} \left[\hat{\mathbf{N}}_\varepsilon^T \mathbf{N}_\sigma \Delta\beta + \hat{\mathbf{N}}_\varepsilon^T \hat{\mathbf{S}} - \hat{\mathbf{N}}_\varepsilon^T \mathbf{N}_\sigma \Delta\beta \right] dA \\
& + \delta\beta^T \int_{\Omega_e} \left[\mathbf{N}_\sigma^T \mathbf{B} \, \Delta\mathbf{v} - \mathbf{N}_\sigma^T \hat{\mathbf{N}}_\varepsilon \, \Delta\alpha + \mathbf{N}_\sigma^T \varepsilon_g - \mathbf{N}_\sigma^T \hat{\mathbf{N}}_\varepsilon \Delta\alpha \right] dA
\end{aligned} \tag{28}$$

where f^a is the load vector which represents external loads. In order to make the formulation more compact we define the following element matrices.

$$\begin{aligned}
\mathbf{K}_g &= \int_{(\Omega_e)} \mathbf{K}_\sigma \, dA & \mathbf{f}^i &= \int_{(\Omega_e)} \mathbf{B}^T \sigma^h \, dA = \mathbf{G}^T \beta \\
\bar{\mathbf{H}} &= \int_{(\Omega_e)} \bar{\mathbf{N}}_\varepsilon^T \mathbb{D} \bar{\mathbf{N}}_\varepsilon \, dA & \mathbf{f}^e &= \int_{(\Omega_e)} \bar{\mathbf{N}}_\varepsilon^T \partial_\varepsilon W \, dA - \mathbf{F}\beta = \begin{bmatrix} \mathbf{f}_1^e \\ \mathbf{f}_2^e \end{bmatrix} \\
\mathbf{F} &= \int_{(\Omega_e)} \hat{\mathbf{N}}_\varepsilon^T \mathbf{N}_\sigma \, dA & \mathbf{f}^s &= \int_{(\Omega_e)} \mathbf{N}_\sigma^T \varepsilon_g^h \, dA - \mathbf{F}^T \alpha \\
\mathbf{G} &= \int_{(\Omega_e)} \mathbf{N}_\sigma^T \mathbf{B} \, dA
\end{aligned} \tag{29}$$

The integrals in (27) and (29) we compute numerically using a 2×2 Gauss integration scheme. With the abbreviations, given in (29), Eq. (28) is written as

$$\begin{aligned}
\delta\Pi_e = {} & \delta\mathbf{v}_e^T \left[\mathbf{G}^T \, \Delta\beta + \mathbf{f}^\mathbf{i} - \mathbf{f}^\mathbf{a} \right] \\
& + \delta\bar{\alpha}^T \left[\bar{\mathbf{H}} \, \Delta\bar{\alpha} \right] - \delta\bar{\alpha}^T \left[\mathbf{F}\Delta\beta + \mathbf{f}^\mathbf{e} \right] \\
& + \delta\beta^T \left[\mathbf{G} \, \Delta\mathbf{v} - \mathbf{F}^T \, \Delta\alpha + \mathbf{f}^\mathbf{s} \right]
\end{aligned} \tag{30}$$

We partition the matrix $\bar{\mathbf{H}}$ into the four matrices $\mathbf{H}, \mathbf{H}_{mz}, \mathbf{H}_{zm}$ and $\mathbf{H}_{zz}$ and separate the components in thickness direction in the matrix $\mathbf{H}_{zz}$.

$$\begin{aligned}
\bar{\mathbf{H}} &= \int_{\Omega_e} \bar{\mathbf{N}}_\varepsilon^T \mathbb{D} \bar{\mathbf{N}}_\varepsilon \, dA = \int_{\Omega_e} \begin{bmatrix} \hat{\mathbf{N}}_\varepsilon & \underline{0} & \underline{0} \\ \underline{0} & \mathbf{N}_\varepsilon^z & \underline{0} \\ \underline{0} & \underline{0} & \tilde{\mathbf{N}}_\varepsilon^{el} \end{bmatrix}^T \mathbb{D} \begin{bmatrix} \hat{\mathbf{N}}_\varepsilon & \underline{0} & \underline{0} \\ \underline{0} & \mathbf{N}_\varepsilon^z & \underline{0} \\ \underline{0} & \underline{0} & \tilde{\mathbf{N}}_\varepsilon^{el} \end{bmatrix} dA \\
&= \begin{bmatrix} \mathbf{H} & \mathbf{H}_{mz} \\ \mathbf{H}_{zm} & \mathbf{H}_{zz} \end{bmatrix}
\end{aligned} \tag{31}$$

Inserting these four matrices in the variational expression leads to

$$\delta\Pi_e = \delta\mathbf{v}_e^T \left[\mathbf{G}^T \, \Delta\beta + \mathbf{f}^\mathbf{i} - \mathbf{f}^\mathbf{a} \right] \tag{32}$$

$$+ \; \delta\alpha^T \left[\mathbf{H} \, \Delta\alpha + \mathbf{H}_{mz} \, \Delta\alpha_{33} - \mathbf{F} \, \Delta\beta + \mathbf{f}^\mathbf{e} \right] \tag{33}$$

$$+ \; \delta\alpha_{33} \left[\mathbf{H}_{zm} \, \Delta\alpha + \mathbf{H}_{zz} \, \Delta\alpha_{33} \right] \tag{34}$$

$$+ \; \delta\beta^T \left[\mathbf{G}^T \, \Delta\mathbf{v} - \mathbf{F}^T \, \Delta\alpha + \mathbf{f}^\mathbf{s} \right] \tag{35}$$

We consider that no continuity for α, α_{33}, β is required between the elements, thus the Eqs. (33) - (35) shall be zero on element level. Solving the system of equations by static condensation of

$\Delta\alpha_{33}$ yields

$$\begin{aligned} \tilde{\mathbf{H}}\,\Delta\alpha - \mathbf{F}\,\Delta\beta + \bar{\mathbf{f}}^{\,e} = \mathbf{0} \qquad & \tilde{\mathbf{H}} = \mathbf{H} - \mathbf{H}_{mz}\,\mathbf{H}_{zz}^{-1}\,\mathbf{H}_{zm} \\ \Delta\alpha_{33} = \mathbf{H}_{zz}^{-1}\,(-\mathbf{f}_2^e - \mathbf{H}_{zm}\,\Delta\alpha) \qquad & \bar{\mathbf{f}}^{\,e} = \mathbf{f}_1^e - \mathbf{H}_{mz}\mathbf{H}_{zz}^{-1}\,\mathbf{f}_2^e \end{aligned} \tag{36}$$

For $\Delta\alpha$ and $\Delta\beta$ results

$$\begin{aligned} \Delta\alpha &= \mathbf{F}^{-T}\,(\mathbf{G}\,\Delta\mathbf{v} + \mathbf{f}^s) \\ \Delta\beta &= \mathbf{F}^{-1}\,(\tilde{\mathbf{H}}\,\Delta\alpha + \bar{\mathbf{f}}^{\,e})\,. \end{aligned} \tag{37}$$

By inserting these two expressions into Eq. (32) arises the following term with the tangential element stiffness matrix $\mathbf{k}_T^e$ and the element residual vector $\hat{\mathbf{f}}$.

$$\begin{aligned} L[\Pi(\theta^h, \delta\theta^h), \Delta\theta^h] &= \sum_{e=1}^{numel} \delta\mathbf{v}^T\,(\mathbf{k}_T^e\,\Delta\mathbf{v} + \hat{\mathbf{f}}) = 0 \\ \mathbf{k}_T^e &= \mathbf{G}^T\,\hat{\mathbf{H}}\,\mathbf{G} + \mathbf{k}_g \qquad \hat{\mathbf{H}} = \mathbf{F}^{-1}\,\tilde{\mathbf{H}}\,\mathbf{F}^{-T} \\ \hat{\mathbf{f}} &= \mathbf{G}^T\,(\beta + \hat{\mathbf{H}}\,\mathbf{f}^s + \mathbf{F}^{-1}\,\bar{\mathbf{f}}^{\,e}) - \mathbf{f}^a \end{aligned} \tag{38}$$

After assembling over all elements

$$\mathbf{K}_T\ \mathbf{V} = \hat{\mathbf{F}}$$
$$\text{with} \quad \mathbf{K}_T = \bigcup_{e=1}^{nelem} \mathbf{k}_T^e;\ \mathbf{V} = \bigcup_{e=1}^{nelem} \mathbf{v}_e;\ \hat{\mathbf{F}} = \bigcup_{e=1}^{nelem} \hat{\mathbf{f}}_e$$

the problem is solved with respect to the nodal degrees of freedom.

Actuator Formulation

The actuator formulation implies a constant value for the difference of the electric potential in thickness direction, as it is in practice. The value for each node is predetermined. On element level the average value of the four nodes of the element is calculated and divided through the negative thickness of the shell.

$$\vec{\mathbf{E}}_{3\,e} = -\frac{1}{4}\sum_{I=1}^{4}\frac{\Delta\varphi_I}{h} \tag{39}$$

So we get the input data for the electric field in thickness direction. This data are used to install the vector α_{33}.
This yields to the modified stiffness matrix $\mathbf{k}_T^e$ and the modified residual vector $\hat{\mathbf{f}}$

$$\begin{aligned} \mathbf{k}_T^e &= \mathbf{G}^T\mathbf{F}^{-1}\mathbf{H}\mathbf{F}^{-T}\mathbf{G} \\ \hat{\mathbf{f}} &= \mathbf{G}^T\left[\beta + \mathbf{F}^{-1}(-\mathbf{H}_{mz}\alpha_{33} - \mathbf{H}\mathbf{F}^{-T}\mathbf{f}^s + \mathbf{f}^e)\right] - \mathbf{f}^a \end{aligned} \tag{40}$$

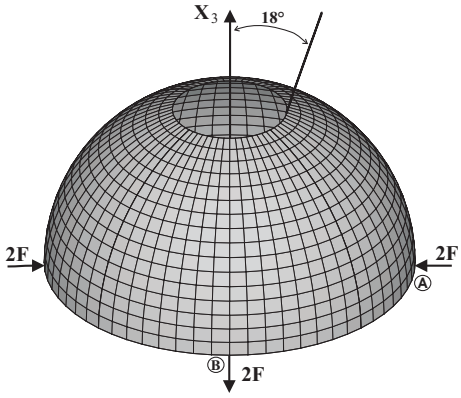

Figure 2. SPHERICAL SHELL WITH CENTER HOLE.

NUMERICAL EXAMPLES

In order to test our finite element formulation, we chose some numerical examples, which demonstrate the ability of the present shell element to analyze piezoelectric devices. The presented element fulfills the important patch tests, membrane, bending and shear test, which have been adopted for coupled field problems.

Spherical Shell

The test of a thin version of the spherical shell (see Figure 2) according to MacNeal and Harder [8] shows good accordance of the results with other elements for the mechanical case. Here the material is short-circuit, so the electrical components are neglected. The doubly curved shell with an 18° center hole has a radius of $R = 10$ and a thickness of $h = 0.01$. The equatorial edge is loaded with four point loads $2F$ alternating in sign at 90° intervals. The structure is fixed in 3-direction at the equator points staggered 45° to the loads. The electric degree of freedom is fixed everywhere. The system is modeled with the material parameters $E = 6.825 \cdot 10^7$ and $\nu = 0.3$. With respect to the symmetry of the system only a quarter of the shell is modeled with 16x16 elements. Figure 3 shows the nonlinear load-displacement curves for point A and point B in comparison with the results of Betsch and Stein [9] , Parisch [10] and Wagner and Gruttmann [6] , which all deploy the same number of degrees of freedom.

Bimorph

Second benchmark test is a cantilever bimorph. This piezoelectric benchmark test verifies the results of the sensor and actuator application of the shell element. The geometry of the bimorph, which consists of two opposite poled piezoelectric PVDF layers, is shown in Figure 4. The geometry and the

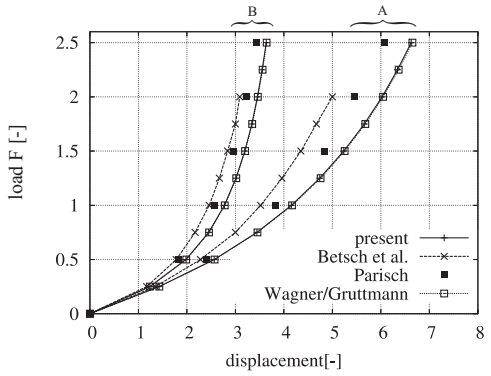

Figure 3. LOAD-DISPLACEMENT BEHAVIOR OF THE SPHERICAL SHELL.

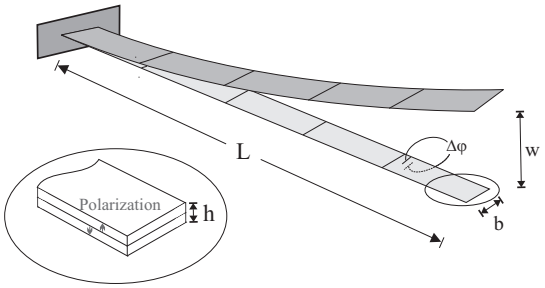

Figure 4. GEOMETRY OF BIMORPH.

Table 1. GEOMETRY AND MATERIAL PARAMETERS FOR BIMORPH.

$L = 0.1m$	$b = 5 \cdot 10^{-3}m$
$h = 2$ x $5 \cdot 10^{-4}m$	$\nu = 0,29$
$E = 2 \cdot 10^{9} \frac{N}{m^2}$	$w = 0.01m$
$e_{13} = -4.6 \cdot 10^{-2} \frac{C}{m^2}$	
$\varepsilon_{33} = 1.062 \cdot 10^{-10} \frac{C^2}{Nm^2}$	

material parameters with the length L, the width b and the thickness h are given in Table 1

For a sensor test the bimorph is deflected by w as shown in Figure 5. As a result of the deformation an electric potential arises. With five elements along the length of the bimoprh, which correspond to five pairs of electrodes, one obtains the staircase function shown in the diagram of Figure 5.

The results are compared with solutions of other finite element formulations for piezoelectric structures. The presented formulation shows quite well accordance to the values of the finite shell element given by Mesecke-Rischmann [11] . Also a step function is given by Hwang an Park [12] for a laminated

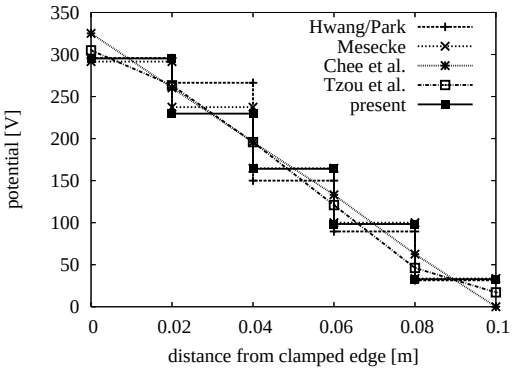

Figure 5. POTENTIAL DISTRIBUTION FUNCTION OF BIMORPH.

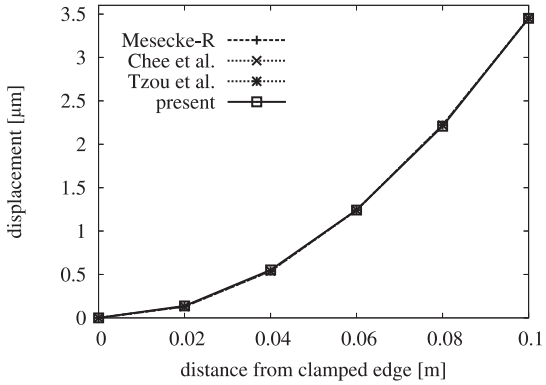

Figure 6. POTENTIAL DISTRIBUTION FUNCTION OF BIMORPH.

plate element. Chee et al. [13] represents a beam element and gives a linear distribution as well as Tzou and Tseng [14] with a shell/plate element.

We can also test the bimorph as an actuator. Therefore we connect a voltage $\Delta\varphi$ on the structure. Due to the opposite polarization, the upper layer becomes shorten and the lower layer elongates. It results a deflection. This deflection depending of the distance of the clamped edge is depicted in the Figure 6. The results of the sensor and the actuator use show good accordance to other piezoelectric finite element formulations. But we remark, that these results are calculated geometrically linear, because of the comparison with the references.

2-Edges Simply Supported Plate

In order to show the significance of a geometrically nonlinear formulation a quadratic plate (see Figure 7) is chosen, which is simply supported in two directions at two edges and subjected to a uniform load Q in the middle between the supports. The

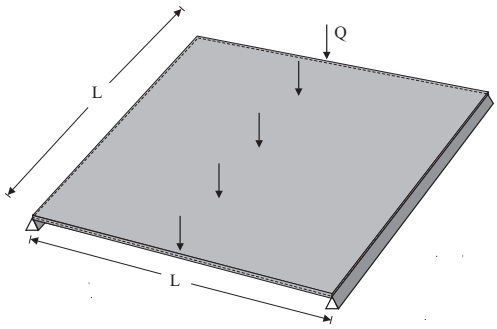

Figure 7. GEOMETRY OF 2-EDGES SIMPLY SUPPORTED PLATE.

Table 2. GEOMETRY AND MATERIAL PARAMETERS FOR 2-EDGES SIMPLY SUPPORTED PLATE.

$E = 67 \cdot 10^9 \frac{N}{m^2}$	$\nu = 0,31$
$L = 0.1m$	$h = 0.5 \cdot 10^{-3}m$
$e_{13} = -9.3 \frac{C}{m^2}$	$\varepsilon_{11} = 1.532 \cdot 10^{-8} \frac{C^2}{Nm^2}$
$e_{15} = 14.57 \frac{C}{m^2}$	$\varepsilon_{33} = 1.532 \cdot 10^{-8} \frac{C^2}{Nm^2}$
$e_{33} = 20.36 \frac{C}{m^2}$	

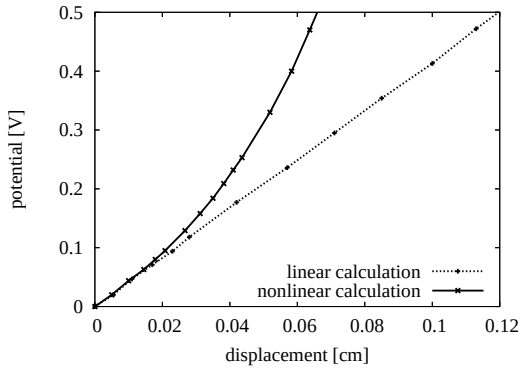

Figure 8. DISPLACEMENT-POTENTIAL-BEHAVIOR OF 2-EDGES SIMPLY SUPPORTED PLATE.

plate has the edge length L and the thickness h. The Young's modulus E, the Poisson ratio ν and the piezoelectric parameters are given in Table 2

Figure 8 shows the curves of the displacement-potential relationship for the linear and the nonlinear calculation. The values of the displacement and the potential in the diagram belongs to the midpoint of the plate. One see the large difference between the curves and thus the significance of the consideration of the nonlinear effect in such systems.

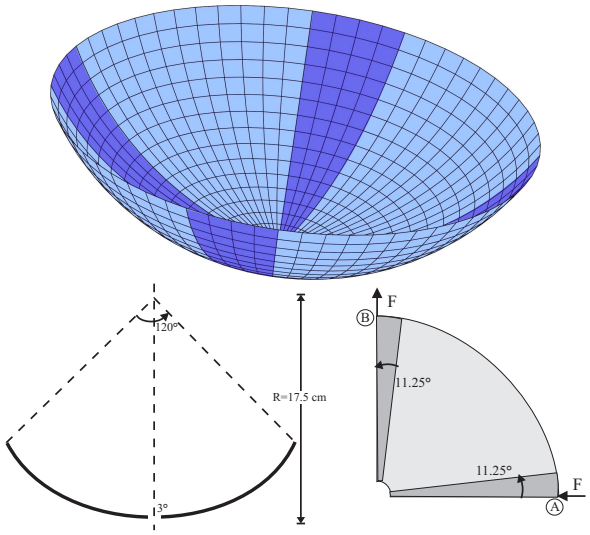

Figure 9. GEOMETRY OF A SMART ANTENNA.

Table 3. GEOMETRY AND MATERIAL PARAMETERS OF SMART ANTENNA.

Aluminium	Piezoelectric segments	
$E = 70 \cdot 10^9 \frac{N}{m^2}$	$E = 67 \cdot 10^9 \frac{N}{m^2}$	$e_{13} = -9.3 \frac{C}{m^2}$
$\nu = 0,3$	$\nu = 0,31$	$e_{15} = 14.57 \frac{C}{m^2}$
$h = 2.03 \cdot 10^{-4}m$	$h = 2.67 \cdot 10^{-4}m$	$e_{33} = 20.36 \frac{C}{m^2}$
	$\varepsilon_{11} = 15.32 \cdot 10^{-9} \frac{C^2}{Nm^2}$	
	$\varepsilon_{33} = 15.32 \cdot 10^{-9} \frac{C^2}{Nm^2}$	

Smart Antenna

As a practical device a smart antenna is presented. The geometry is taken from Gupta et al. [15]. The system consists of an aluminium spherical shell with four integrated piezoelectric segments. The radius of the shell is $R = 17.5\ cm$ with an apex angle of 120°. In the center of the shell there is a small hole of 3°. The system and the geometry are described in Figure 9.

The four piezoelectric segments have an angle of 22.5° each and are arranged isochronous. The material parameters are given in Table 3.

The antenna is subjected to four point loads F, alternating in sign, at every equatorial midpoint of the piezo segment. The load-displacement diagram is depicted in Figure10. It is remarked, that only the displacement in load direction is

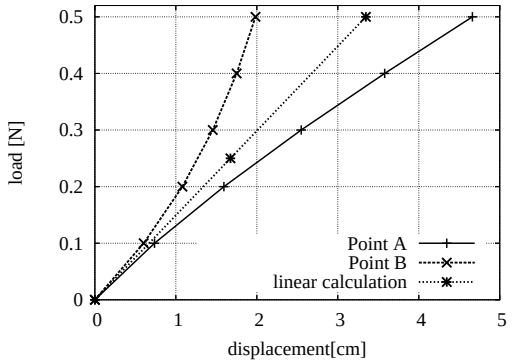

Figure 10. LOAD-DISPLACEMENT-BEHAVIOR OF SMART ANTENNA.

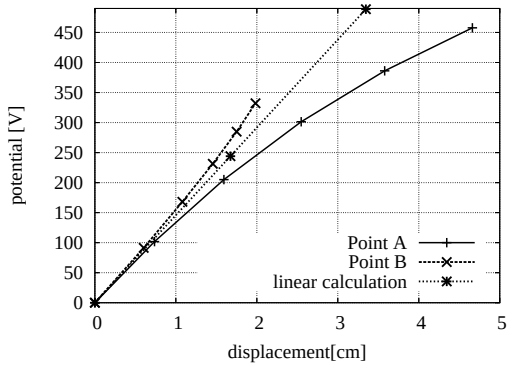

Figure 11. POTENTIAL-DISPLACEMENT-BEHAVIOR OF SMART ANTENNA.

considered. The diagram shows the simulated behavior of the antenna under consideration of geometrical nonlinearity for the point A and B in comparison with a linear calculation. To control the range of the antenna we are interested in the potential-displacement behavior of the structure. Figure 11 shows the potential-displacement results due to a load up to 0.5 Newton. The distinctive nonlinearity brings about larger electric signals for point A than for point B.

In order to manipulate the range of the antenna the indirect piezoelectric effect can be used. Thus by impressing a voltage on the piezo segments the coverage area changes. When we apply the same voltage to all piezo segments, point A and B move outwards or inwards symmetrically (depending on sign). For a difference of the electric potential $\Delta\varphi = 300V$ a displacement of $6.5 \cdot 10^{-3} mm$ at point A and B along the center lines is observed. Applying $\Delta\varphi = 300V$ to the segment of point A and $\Delta\varphi = -300V$ to the segment of point B the shape of the antenna changes as depicted in Figure 12 for a cut through point A. The values of

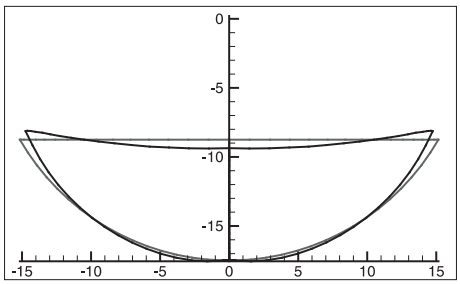

Figure 12. DEFORMATION OF ACTUATED SMART ANTENNA.

displacement in the figure are scaled by factor 200. For point A we observe a displacement of $-2 \cdot 10^{-2} mm$ while point B shows a displacement of $2 \cdot 10^{-2} mm$.

CONCLUSION

Here we presented a piezoelectric finite shell element. The hybrid formulation shows good results for the mechanical and electrical benchmark tests. With only one electrical degree of freedom, we are able to simulate the behavior of both piezoelectric sensor and actuator systems appropriately. The test of the geometrically nonlinear formulation by numerical examples demonstrates the significance of the consideration of the geometrical nonlinearity.

REFERENCES

[1] Klinkel, S., and Wagner, W., 2006. "A geometrically non-linear piezoelectric solid shell element based on a mixed multi-field variational formulation". *International Journal for Numerical Methods in Engineering,* **65**(3), pp. 349–382.

[2] Koegel, M., and Bucalem, M., 2003. "Locking-free piezoelectric MITC shell elements". *Computational Fluid and Solid Mechanics*, pp. 392–395.

[3] Bernadou, M., and Haenel, C., 2003. "Modelization and numerical approximation of piezoelectric thin shells part2: approximation by finite element methods and numerical experiments". *Computer Methods in Applied Mechanics and Engineering,* **192**, pp. 4045–4073.

[4] Voigt, W., 1910. *Lehrbuch der Kristallphysik*. Teubner-Verlag, Leipzig.

[5] Gruttmann, F., and Wagner, W., 2006. "Structural analysis of composite laminates using a mixed hybrid shell element". *Computational Mechanics,* **37**, pp. 479–497.

[6] Wagner, W., and Gruttmann, F., 2005. "A robust non-linear mixed hybrid quadrilateral shell element". *Int. Journal for Numerical Methods in Engineering,* **64**, pp. 635–666.

[7] Simo, J., and Hughes, T., 1998. *Computational Inelasticity*. Springer-Verlag, New York, Berlin, Heidelberg.

[8] MacNeal, R., and Harder, R., 1985. "A proposed standard set of problems to test finite element accuracy". *Finite Elements in Analysis and Design,* **1**, pp. 3–20.

[9] Betsch, P., and Stein, E., 1995. "An assumed strain approach avoiding artificial thickness straining for a nonlinear 4-node shell element". *Commun.Numer. Methods Engrg.,* **11**, pp. 899–909.

[10] Parisch, H., 1995. "A continuum-based shell theory for non-linear applications". *Int. J. Numer. Methods Engrg.,* **38**, pp. 1855–1883.

[11] Mesecke-Rischmann, S., 2004. "Modellierung von flachen piezoelektrischen schalen mit zuverlässigen finiten elementen". PhD thesis, Helmut-Schmidt-Universität, Hamburg.

[12] Hwang, W., and Park, H., 1993. "Finite element modeling of piezoelectric sensors and actuators". *AIAA Journal,* **31**(5), pp. 930–937.

[13] Chee, C., Tong, L., and Steven, G., 1999. "A mixed model for composite beams with piezoelectric actuators and sensors". *Smart Material and Structures,* **8**, pp. 417–432.

[14] Tzou, H., and Tseng, C., 1991. "Distributed vibration control and identification of coupled elastc/piezoelectric systems: Finite element formulation and application". *Mechanical Systems and Signal Processing,* **5**(3), pp. 215–231.

[15] Gupta, V., Seshu, P., and Issac, K. K., 2004. "Finite element and experimental investigation of piezoelectric actuated smart shells". *AIAA Journal,* **42**(10), pp. 2112–2123.